Proceedings World Geothermal Congress 2026
Calgary, Canada, June 8 – 11, 2026

Using Dense Arrays Of Seismic Nodes To Image The Geothermal System On The Island Of Montserrat

J Michael Kendall[1]*, Bogiatzis P[1], Kounoudis R[1], Mackay-Champion T[1], Chow J[1], Shams S[1], Ryan G A[2,3], Williams B A C[2] and Blundy J[1]

University of Oxford, Department of Earth Sciences, UK[1]*, Montserrat Volcano Observatory, Flemmings Montserrat[2], Seismic Research Centre, The University of the West Indies, Trinidad and Tobago[3]

mike.kendall@earth.ox.ac.uk

Keywords: Montserrat, seismic imaging, seismicity, seismic nodes, exploration, imaging.

ABSTRACT

The Soufrière Hills Volcano on Montserrat, in the Lesser Antilles, experienced five eruptive phases between 1995 and 2010, causing devastation in the southern part of the island. Since then, the island has been rebuilding with a focus on decarbonization and geothermal energy. Over a decade ago, three exploration wells were drilled, revealing geothermal potential exceeding the island's energy needs. In 2024, the University of Oxford, funded by the Oxford Martin School and in collaboration with the Montserrat Volcano Observatory (MVO), launched a new geophysical campaign to expand previous geophysical surveys and deepen geothermal exploration. The MVO's broadband seismic network has been augmented to 16 instruments, and 120 Sercel WiNG seismic nodes were deployed in key locations. These nodes significantly enhance the resolution of both seismic activity and passive imaging techniques such as tomography. The project uses volcano-tectonic earthquakes and ambient noise imaging to map three-dimensional compressional and shear wave velocity structures. Finite frequency sensitivity kernels are applied in place of traditional ray paths to better reflect realistic data sensitivity. Results show notable seismic velocity anomalies associated with volcanic and geothermal features. High P-wave velocities are observed beneath Soufrière Hills and the older Centre Hills volcanic centres. A pronounced low-velocity anomaly appears west of the Island, aligned with the site of previously drilled high-temperature geothermal wells. This feature extends laterally, and is detectable down to approximately 3.5 km depth, complimenting previous geophysical surveys and together offering valuable insight into the island's geothermal potential.

1 INTRODUCTION

The Caribbean region has some of the highest electricity prices globally, despite possessing substantial untapped geothermal energy potential. Montserrat, in particular, experiences some of the highest electricity costs in the Caribbean, yet its estimated geothermal resource exceeds 50 MW and may be 100s MW (Montserrat Energy Policy 2008–2027; Ryan, 2016). Three exploratory wells (MON-1 and MON-2 drilled in 2013, and MON-3 in 2016) revealed a geothermal potential ≥2 MWe, sufficient to meet the island's current energy demand. However, high capital investment requirements for power plant development and necessary grid infrastructure upgrades have impeded progress.

Montserrat's geothermal potential arises directly from its tectonic and volcanic setting – volcanoes give and they take. The island hosts four volcanic centres that decrease in age from north to south: Silver Hills, Centre Hills, Soufrière Hills, and South Soufrière Hills. After approximately 350 years of dormancy, the Soufrière Hills Volcano reawakened in 1995, and the last of five eruptive phases ended in 2010 (Wadge et al., 2014). The eruption sequence caused widespread devastation, including the evacuation and destruction of the capital, Plymouth, and the establishment of an exclusion zone on the southern half of the island. In response, the Montserrat Volcano Observatory (MVO) was established in 1995 to monitor volcanic activity. A seismic network, rapidly deployed during the initial eruption, has been in continuous operation since, yielding one of the longest sustained volcano monitoring datasets worldwide. These data are invaluable not only for assessing volcanic hazards, but also for improving understanding of Montserrat's geothermal system.

The exploratory drilling campaign demonstrated considerable geothermal potential. Static BHTs of 230 °C in MON-1 at 2298 m depth, 265°C in MON-2 at 2870 m and 186 °C at 2286 m in MON-3 were recorded. Integrating magnetotelluric resistivity measurements, earthquake hypocentre distributions, and a three-dimensional P-wave velocity model, Ryan et al. (2013) proposed a high-temperature, fracture-controlled geothermal system located at the intersection of two faults in the island's southwest. Ryan and Shalev (2014) also proposed a three-dimensional estimation of geothermal reservoir temperatures using the correlation between anomalies in P-

wave seismic velocity and geothermal well log temperatures. Comparable reservoirs, including deeper supercritical systems, may exist elsewhere on the island.

In 2024, the Oxford Martin School launched the *ReSET* (rethinking natural resources) project to reassess Montserrat's geothermal potential and explore the co-recovery of critical metals from geothermal fluids. Deep, supercritical hypersaline fluids in volcanic environments represent a promising source of economically valuable metals (Blundy et al., 2021). The programme unites researchers across disciplines to examine the island's coupled geophysical, geochemical, and socio-economic dimensions. The geophysical component, led jointly by the University of Oxford and the MVO, aims to better delineate Montserrat's geothermal systems. A key element of this effort is the deployment of 120 portable seismic nodes across the island. Here, we present the advantages of nodal seismic networks for geothermal exploration and summarize preliminary results from the ongoing seismic campaign.

2 SEISMIC ARRAY AND DATA

Seismic monitoring is one of the most widely used tools in volcano research and hazard assessment. It provides insights into the movement of magma, volcanic fluids, and tectonic stresses beneath a volcano. These signals can also be used to image geothermal systems, offering information complementary to those obtained from electrical and electromagnetic methods.

Conventional seismic monitoring typically relies on semi-permanent short-period or broadband seismometers, with broadband instruments preferred as they capture a wider range of seismic signals. In recent years, the development of low-cost, easily deployable sensors has enabled the rapid installation of hundreds of seismic nodes, making dense array studies feasible - an approach ideally suited to geothermal investigations (e.g., Hudson et al., 2024).

As part of the *ReSET* project in 2024, the University of Oxford and the Montserrat Volcano Observatory (MVO) deployed nearly 120 Sercel WiNG Digital Field Units (DFUs) (Figure 1). The WiNG node is a compact, MEMS-based broadband sensor designed for ease of deployment and extended battery life (up to approximately 50 days). Although each unit records a single vertical component, nodes can be installed in a 3-component Galperin configuration, allowing full waveform analysis. The WiNG's portability, durability, and excellent low-frequency response make it particularly valuable for volcano and geothermal monitoring in remote, rugged terrain.

Between May 2024 and December 2025, three WiNG deployment campaigns were conducted on Montserrat (May–July 2024, October–December 2024, and October–December 2025). Data processing and interpretation are ongoing, but this paper presents preliminary results from the first campaign in early 2024, which focused on increasing station density in the northern part of the island.

A semi-linear array of nodes was installed near the geothermal test wells MON-1, MON-2, and MON-3 (Figure 1). A north–south profile was established during the first campaign (May–July 2024), followed by an east–west profile later that year. The project also investigates the use of dense nodal arrays for beamforming and microseismic event detection, similar to the approach described by Hudson et al. (2024). Two arrays, each consisting of 18 sensors arranged in two concentric rings around a central node, were deployed on the eastern and western margins of the exclusion zone (Figure 1); these datasets are still under analysis.

In addition, the *ReSET* campaign installed eight broadband Güralp Certimus sensors in May 2024 (Figure 1). These instruments augment the permanent MVO seismic network, with several providing real-time data transmission to the observatory. Powered by solar panels, the Certimus instruments have operated continuously since deployment, offering valuable complementary broadband coverage to the MVO permanent array and the temporary nodal arrays.

3 RESULTS

3.1 Earthquake detection and location methodology

Data from the combined network of nodes and broadband seismograph stations were used to detect and locate seismic events across Montserrat using QuakeMigrate, a microseismic detection algorithm (Hudson et al., 2024; Yemane et al., 2025). Prior to analysis, the raw seismic waveforms from each station were bandpass filtered between 2 and 20 Hz.

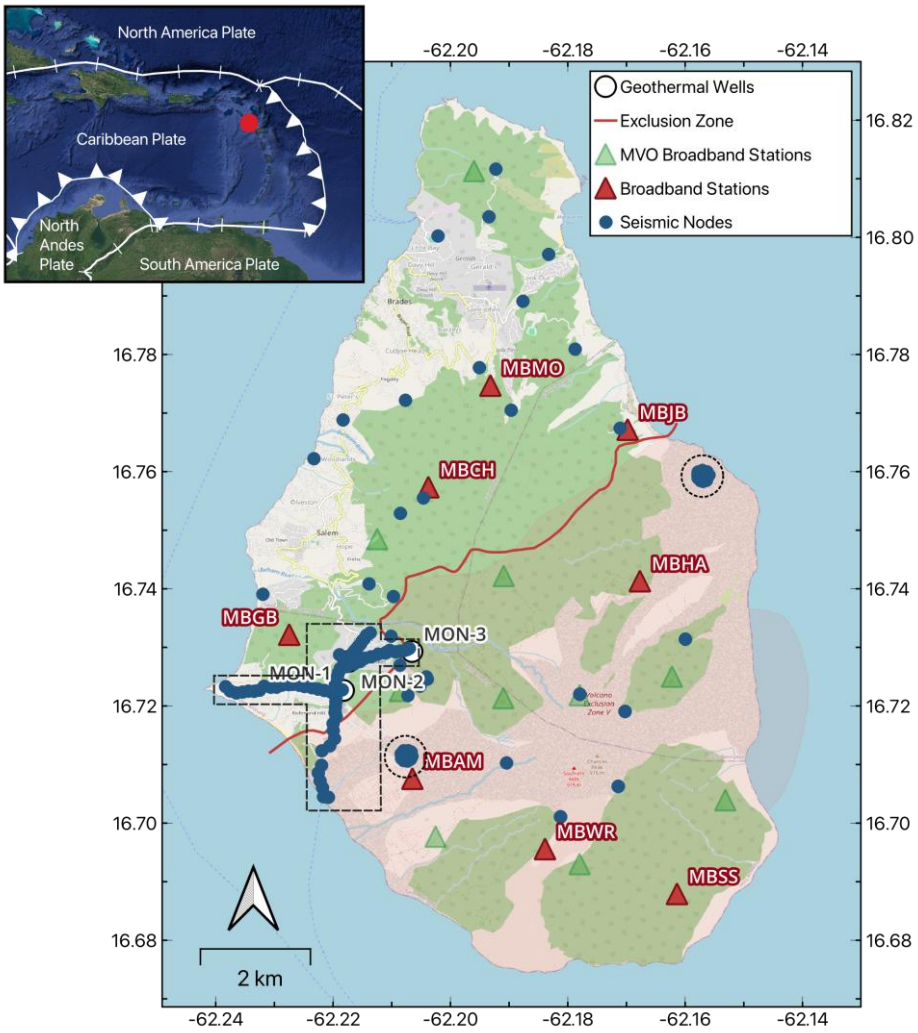


Figure 1. A map of seismic stations on the island of Montserrat. Red triangles denote the MVO permanent stations, green triangles show the locations of the *ReSET* broadband stations. The blue circles show the locations of 120 seismic nodes. The majority are deployed in a tight configuration around the geothermal test wells, MON1, MON2 and MON3 (white circles). Arrays of 18-element seismic nodes are shown by blue circles surrounded by dashed lines in regions to the east of west of the island and south of the border of the exclusion zone. The map inset at the top left of the figure shows the location of Montserrat in the Lesser Antilles Arc.

QuakeMigrate performs a continuous scan through time using a pre-defined 3D grid (i.e., a Look-Up Table, LUT) of theoretical travel times for P and S phases for each station in the network. At each grid node and time step, the algorithm evaluates where and when the observed seismic waveforms best coalesce – i.e., where signals from multiple stations align in time according to the LUT predictions. This is done by computing an onset function based on the Short-Term Average/Long-Term Average (STA/LTA) ratio to estimate the likelihood of a phase arrival at each time step; we used an STA of 0.2s and LTA of 1.0s. These onset likelihoods are then migrated back into the 3D LUT grid and stacked across all recording stations to produce a coalescence function. The resulting coalescence function represents the likelihood of an event having occurred at each time step. Where both P- and S-phase onset functions are available (i.e., in the broadband stations), they are combined in the generation of the coalescence trace. An event is triggered when the normalised coalescence energy at a particular point in 3D space at a given time is very high and expected to exceed noise levels.

For each triggered event, the migration process is re-run over a refined, high-resolution 3D LUT grid to allow for a more accurate estimation of the event's origin time and hypocentral location and for the production on phase picks (arrival times for both P and S) derived from the back-projected maxima. These preliminary picks are then passed on to the NonLinLoc (NLL) algorithm stage for formal probabilistic relocation.

Figure 2 shows a comparison of seismicity identified and located using only the exiting 8 element MVO array and the new *ReSET* array for a 2-month time period. Unsurprisingly, the *ReSET* array detects more events, over more of the island and has a lower detection threshold.

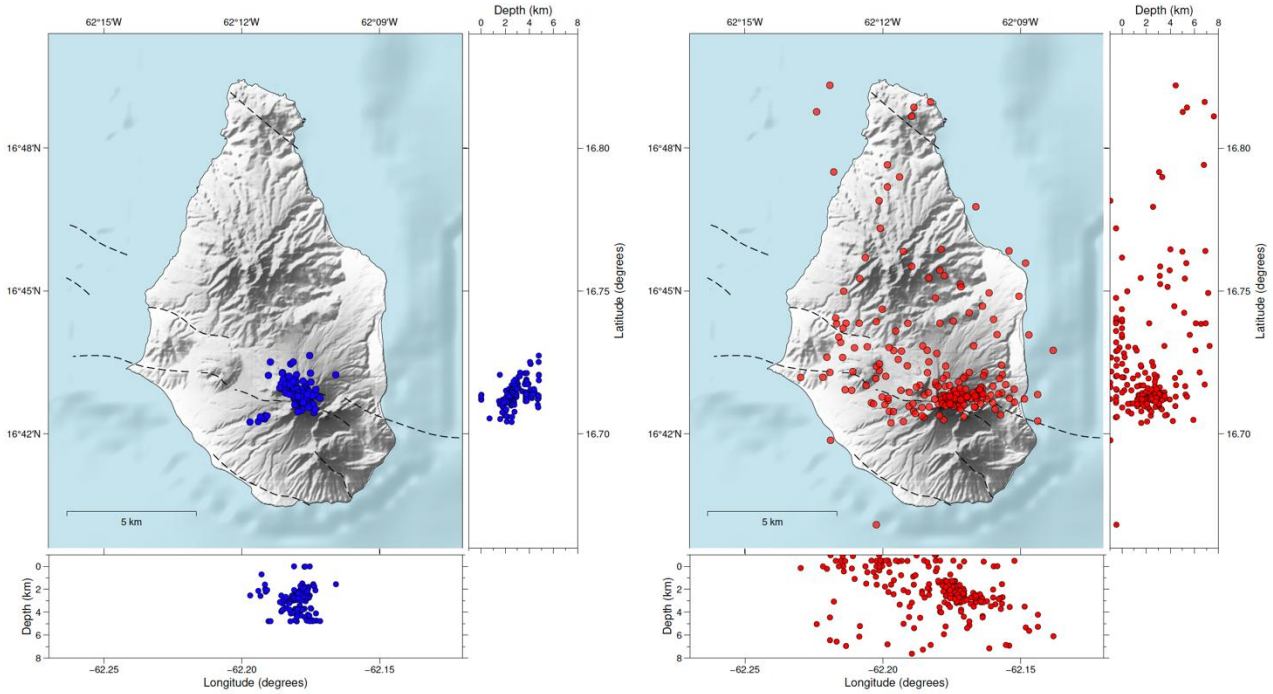


Figure 2. Seismicity recorded in the time period of 30th May 2024 to 24th October 2024. The left shows events (blue dots) recorded and located by the MVO observatory stations (see Figure 1). The right (red dots) show events recorded with the full complement of permanent seismic stations and seismic nodes, as shown in Figure 1. For August to October 2024, only the broadband stations (MVO network and new ReSET Certimus stations), were used for earthquake detection. Depth profiles show to the right and beneath the map show the distribution of the events in depth.

3.2 Seismic travel-time tomography

The recorded seismicity can be used to image the subsurface structure of Montserrat's geothermal system. To start we show seismic tomographic images using legacy data. We then show the added improvement in resolution and uncertainty due to the extra broadband stations and the seismic nodes. Here we focus on the use of P-waves to image the seismic velocity structure.

The first dataset consists of 7112 P-wave arrivals from 1039 mostly volcano-tectonic/tectonic earthquakes occurring between 1996-2007 and recorded at up to 23 stations of the Montserrat Volcano Observatory (MVO) and manually repicked by Baird et al. (2015). Only events with at least four P arrivals are considered. The second dataset is augmented with 5491 additional P-wave arrivals from 133 new events that occurred between May and September of 2024, detected from the combination of the MVO network, 8 Certimus broadband stations and 98 Sercel WiNG nodes.

A rectangular grid, defined in a local vertical Cartesian coordinate system, with origin the peak of SHV projected at 0 m elevation is used as the inversion grid, for the P-wave model. The spacing varies from ~300m beneath the island up to ~6km depth to ~ 1km at the edges of the model. Finer spacing of ~100 m accommodates for the topography above sea level. The forward problem is solved by means of the shortest path method (Bogiatzis et al., 2019) in a refined completely unstructured grid, regenerated in each iteration using the JIGSAW mesh generator (Engwirda, 2018), to avoid systematic error propagation in travel time calculations (Bogiatzis et al., 2021). The topography (Copernicus DEM, 2022) and bathymetry (GEBCO, 2025) are explicitly introduced in the forward grid as fixed points, and the velocities are fixed in air and sea accordingly. To accommodate finite frequency effects the length of the geometrical ray path is distributed within the first Fresnel volume with linear weights (Liu et al., 2009; Watanabe et al., 1999). Dominant frequencies were set at 5Hz for P-wave arrivals by frequency analysis of a subset of the data.

A nonlinear, joint inversion scheme is utilized that inverts simultaneously for P-wave slowness' and hypocentre corrections, by expanding the misfit functions using Taylor series about a 1-D starting model similar to the ocean model of (Shalev et al., 2010) and the initial locations of earthquakes (Baird et al., 2015). A multi-objective minimization function is set, which in addition to P-wave residuals, penalizes the cross-product of the slowness gradients of the two models (Gallardo & Meju, 2004; Hu et al., 2009) ensuring structural similarity of the results. Additional Tikhonov regularization of 0^{th} (damping) and 2^{nd} order (Laplacian) is applied to stabilize the inversion and reduce unnecessary structure that is not required by the data (Aster et al., 2013). The inversion is carried out using direct sparse methods and in particular the Cholesky decomposition (Chen et al., 2009), allowing the calculation of the resolution matrix and therefore the assessment of the robustness of the imaged features (Bogiatzis et al., 2016, 2019).

Figure 3 shows a depth cross-section of the P-wave velocity structure in a transect across the southern part of the island. This is based on only the legacy seismicity data (Baird et al., 2015). Warm colours show low seismic velocities and cold colours show higher seismic velocities.

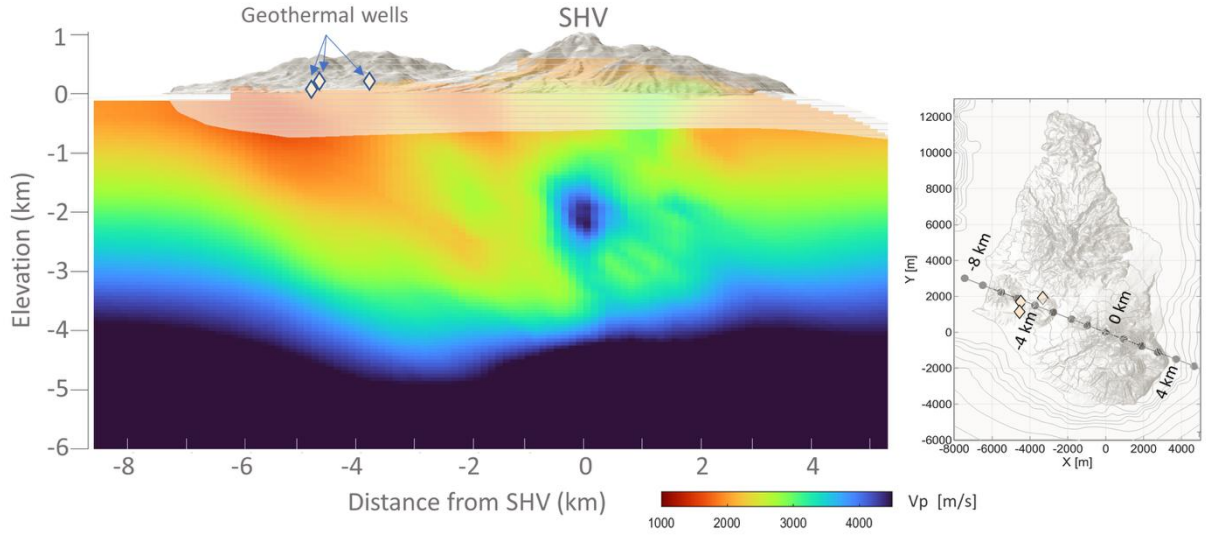


Figure 3. The P-wave velocity structure in an ESE-WNW direction across the southern part of Montserrat (as shown in the inset). The location of the Soufrière Hills volcano (SHV) is shown, as the three geothermal wells, MON1, MON2 and MON3.

Figure 4 shows how the addition of the *ReSET* instruments (nodes and broadband seismometers) improve the seismic resolution and uncertainties in seismic velocities. The results illustrate the improved imaging in the north parts of the island, which is a result of a wider distribution of events.

3.3 Ambient noise tomography

Seismic ambient noise tomography (ANT) is a technique that uses continuous background seismic vibrations - generated for example by ocean waves, wind, and human activity - to image the Earth's subsurface without the need for active sources or earthquakes. By cross-correlating ambient noise recorded at pairs of seismic stations, surface wave travel times can be extracted and inverted to produce three-dimensional velocity models. When applied to volcanoes, ANT provides valuable constraints on shallow crustal structure, helping to delineate magma storage zones, hydrothermal systems, and regions of altered or fractured rock associated with volcanic activity. Given the size of Montserrat, ANT can only image down to depths of roughly 3-4 kilometers.

Cross-correlations of the seismic node data are calculated for each possible station pair. Pre-processing involved detrending, 1-bit normalization and spectral whitening following Bensen et al. (2007), followed by down-sampling the data to 20 Hz. The time-series were binned into 1hr-long files for the calculations. Average cross-correlations for each station-pair were calculated using a signal-to-noise stacking routine, in which a linear stack was taken while using the signal-to-noise value as a weighting. Following this, cross-correlations with signal-to-noise values below 3 were discarded. Figure 5a shows cross-correlations (filtered between 0.1-2 Hz) as a function of station-pair offset. Rayleigh wave moveout is clearly visible.

For each frequency of interest, the average surface-wave phase velocity across the network was determined by identifying the velocity that minimized the residual between the observed phase of the real (symmetric) component of the cross-correlations and the theoretical phase derived from the zero-order Bessel function of

the first kind - a component of the empirical Green's function for surface waves (Sánchez-Sesma & Campillo, 1991). The total phase for each station pair was then estimated by unwrapping the phase of the Fourier-transformed cross-correlations, using the previously determined average phase velocity as an initial estimate of the number of wavelengths between stations.

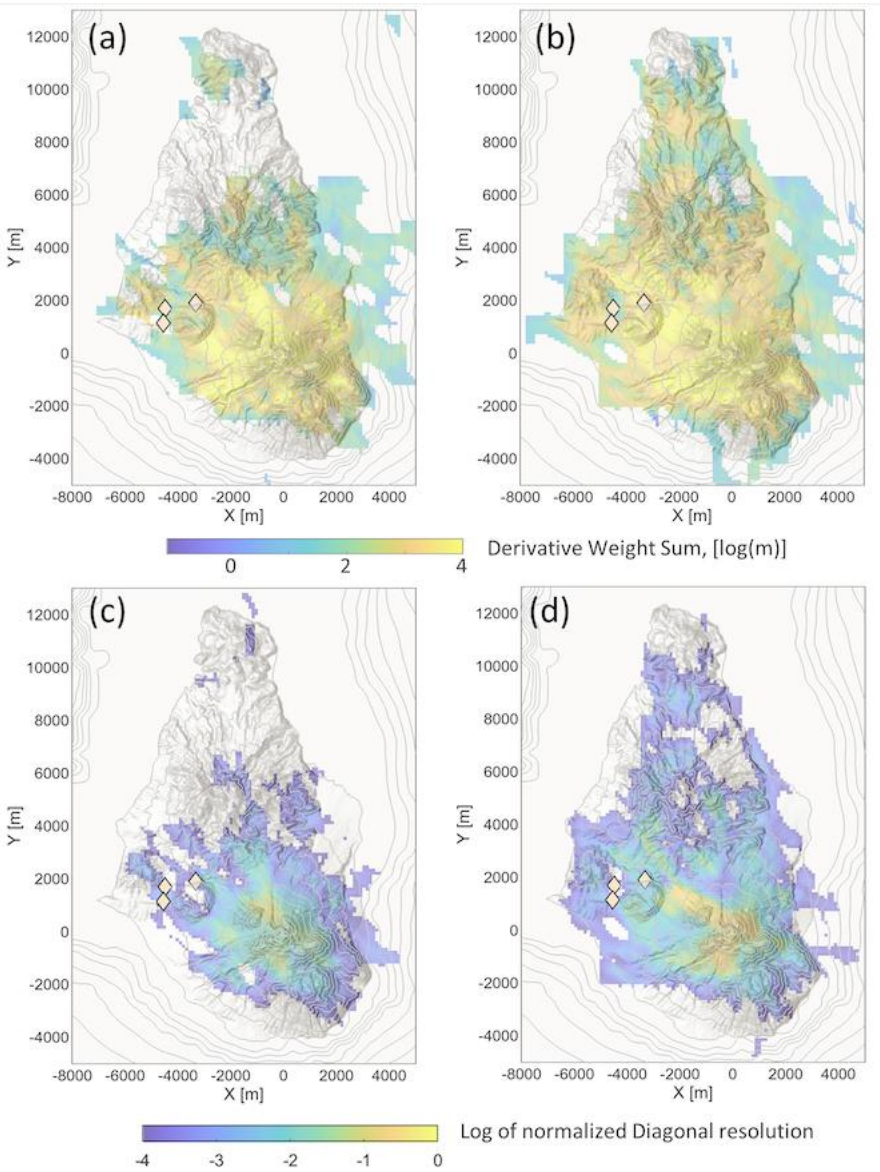


Figure 4. Sensitivity and resolution enhancement with the increased number of seismic stations. Top row: Comparison of the Derivative Weight Sum (DWS) at the depth 1500 m below sea level for (a) from the dataset of Baird et al. (2014) and (b) the new combined dataset that includes the data from the *ReSET* deployment. DWS represents the combined length of every ray path that affects each model parameter and is computed by summing the elements of the Jacobian matrix column-wise. Significant improvements in sensitivity are apparent throughout the island and especially at the central and northern parts. The Bottom row compares of the diagonal elements of the model resolution matrix, normalized with the maximum value of the resolution matrices of the two datasets. Diagonal resolution quantifies how well each model parameter can be independently recovered from the available data. (c) and (d) corresponds to the datasets mentioned for (a) and (b), respectively.

Finally, the total phases from all usable station pairs were inverted to produce network-wide two-dimensional phase-velocity maps using an iterative, damped, weighted least-squares inversion following Forsyth and Lin (2005) (Figure 5b).

4 INTERPRETATION

The addition of a large number of seismic nodes to the monitoring network has substantially increased coverage of seismicity beneath Montserrat and significantly lowered detection thresholds. As expected, the majority of events remain concentrated beneath the Soufrière Hills Volcano (Figure 2); however, the *ReSET* array identifies additional earthquakes that further delineate an eastward-trending cluster beneath the edifice. The new stations also detect seismic activity across the entire island, including notable events beneath the older Centre Hills and Silver Hills volcanoes. Moreover, the *ReSET* array records deeper events than the existing MVO network, likely due to its enhanced sensitivity and lower detection threshold.

Seismic P-wave tomography reveals high-velocity mafic material emplaced beneath the Soufrière Hills Volcano (Figure 3). A small pocket of high-velocity material directly beneath the volcano at 2 km depth likely represents partially solidified magma associated with the recent eruption and connected to the deeper system by thin, dyke-like tendrils of higher velocity. The tomographic image also indicates crustal loading associated with the volcanic complex, depressing the regional > 4 km s^{-1} velocity contour. A pronounced low-velocity zone is evident beneath the area encompassing the three geothermal wells (MON1-3), consistent with the location of high-temperature geothermal reservoirs. Comparable low-velocity anomalies are observed to the east and west of the volcano. Similar structural patterns were imaged in the SEA-CALIPSO experiment (Shalev et al., 2010), which used airgun sources and onshore geophone arrays; however, the new earthquake-derived tomographic images provide improved structural clarity and resolution.

Figure 4 demonstrates that the new seismicity detected by the *ReSET* nodal array will significantly enhance imaging of the northern part of the island. The next phase of this work involves constructing updated tomographic models using the expanded *ReSET* seismicity catalogue.

Finally, using ANT, the dense nodal array greatly improves resolution of the shallow velocity structure across Montserrat. Low-velocity anomalies near the geothermal test wells are clearly shown in Figure 5b. The phase-velocity map, derived at 1 Hz, is sensitive to depths of approximately 1–1.5 km and thus provides detailed imaging of the shallow subsurface (< 2 km). Consequently, the ambient noise tomography (ANT) results complement the earthquake travel-time tomography by resolving near-surface structures that are otherwise poorly constrained. A key next step is to integrate the shallow ANT models with the deeper travel-time tomographic results (Figures 3 and 4) to produce a comprehensive 3D model of Montserrat's crustal and geothermal structure.

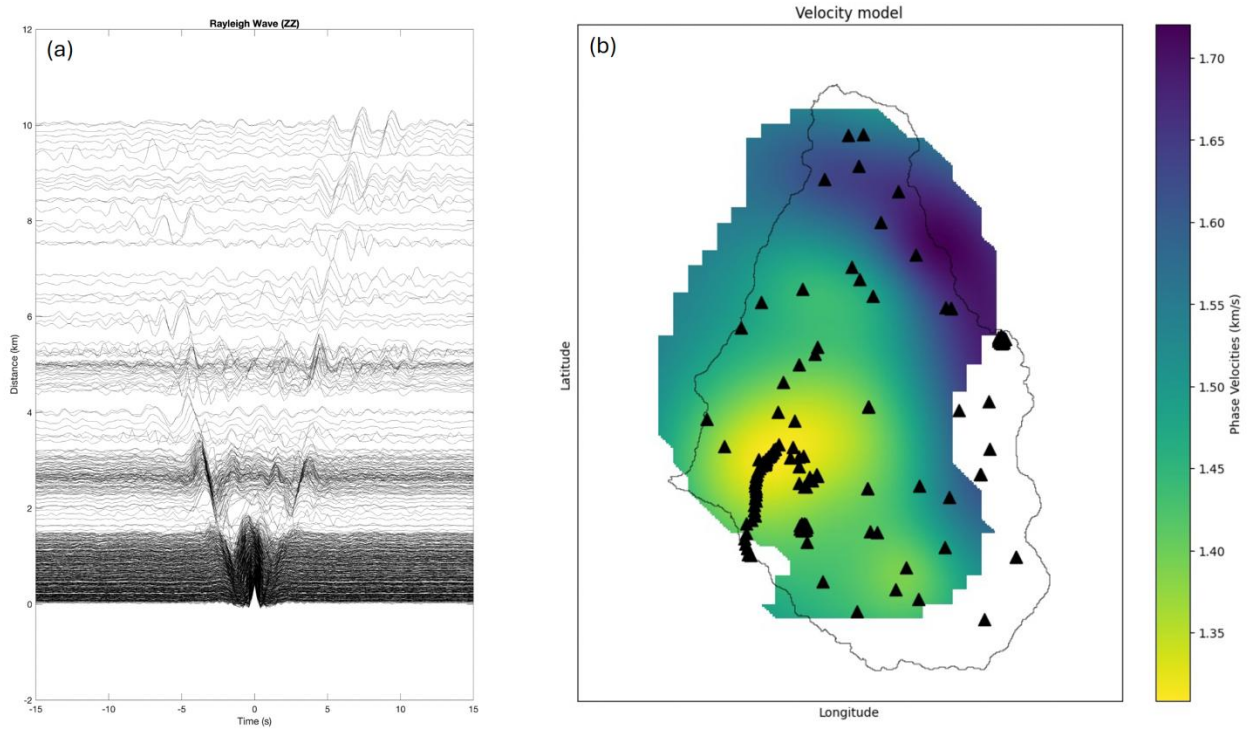


Figure 5. (a) Cross-correlations as a function of station-pair offset. The cross-correlations are filtered between 0.1-2Hz. (b) Phase velocity map for a 1Hz Rayleigh-wave. Velocity uncertainty is ~0.05 km/s.

5 CONCLUSIONS AND FUTURE DIRECTIONS

Preliminary results from the deployment of a dense array of nodal seismometers on the island of Montserrat demonstrate the strong potential of this approach for resolving volcanic systems and geothermal reservoirs with greater detail than conventional sparse networks. The installation of 120 seismic nodes, complemented by eight broadband sensors, has augmented the Montserrat Volcano Observatory (MVO) monitoring network, reducing seismic event detection thresholds and expanding spatial coverage across the island. Such temporary, high-density arrays offer considerable promise for geothermal exploration, including the detection and characterization of deeper supercritical reservoirs that may host metalliferous fluids.

The enhanced network records seismicity throughout the island, enriching the MVO earthquake catalogue. P-wave travel-time tomography using these events reveals the internal structure of geothermal reservoirs and magmatic intrusions, while the improved data density from the nodal array enhances resolution and reduces uncertainty in tomographic models. Ambient noise tomography (ANT) further complements these analyses by providing detailed imaging of the shallow subsurface (< 3 km). Joint inversions of ANT images and earthquake travel-time tomographic images will allow a more comprehensive characterization of shallow geothermal systems and their connection to deeper magmatic sources.

Despite these scientific advantages, the deployment of dense nodal arrays presents several logistical challenges. The Sercel WiNG nodes require recharging approximately every 50 days, necessitating a sustained field presence. Locating buried or camouflaged instruments can also be difficult in Montserrat's tropical environment, where vegetation grows rapidly; in this study, metal detectors were used to aid retrieval. In addition, the large data volumes generated by such deployments demand robust data management, storage, and processing strategies to ensure timely analysis and integration with existing monitoring datasets.

Our results indicate the presence of additional geothermal reservoirs across Montserrat, suggesting that the island possesses significantly greater geothermal energy potential than required for domestic consumption. This surplus capacity enhances the commercial attractiveness of Montserrat's resources to geothermal development companies. The *ReSET* project is exploring options for utilizing excess thermal energy, including co-location of industry close to the MON wells. In parallel, the project is assessing the metal content of Montserrat's geothermal brines, as the co-recovery of heat and critical metals could improve the economic viability and sustainability of geothermal development on the island (Blundy et al., 2021).

In conclusion, the use of dense arrays of seismic nodes holds much potential for geothermal exploration, especially when combined with other exploration techniques such magnetotellurics and/or gravity, which have different sensitivities to sub-surface materials. Furthermore, seismic nodes will be very useful in rapid field deployments during times of seismo-volcanic unrest, providing a hazard monitoring tool.

Acknowledgements

The *ReSET* programme gratefully acknowledges generous funding from the Oxford Martin School. We also thank the Montserrat Volcano Observatory (MVO), the Government of Montserrat, and the UK Foreign, Commonwealth and Development Office (FCDO) for their invaluable support. Additional funding was provided through an Institutional NERC International Science Partnership Fund (ISPF) ODA Grant (KCD00150 – DG01). JC acknowledges support from a Rio Tinto DPhil Scholarship, and SS received fieldwork funding from St Edmund Hall, University of Oxford. JB is supported by a Royal Society Research Professorship.

REFERENCES

Aguilera Bustos, J. P., and Adam, L.: Experimental insights into factors influencing Vp/Vs ratios at the Nevado del Ruiz Volcano, Colombia, *Volcanica*, **6**, 283 299, https://doi.org/10.30909/vol.06.02.283299, 2023.

Aster, R. C., Borchers, B., and Thurber, C. H.: *Parameter Estimation and Inverse Problems*, Elsevier, https://doi.org/10.1016/C2009-0-61134-X, 2013.

Baird, A. F., Kendall, J.-M., Sparks, R. S. J., and Baptie, B.: Transtensional deformation of Montserrat revealed by shear wave splitting, *Earth Planet. Sci. Lett.*, **425**, 179–186, https://doi.org/10.1016/j.epsl.2015.06.006, 2015.

Bensen, G. D., Ritzwoller, M. H., Barmin, M. P., et al.: Processing seismic ambient noise data to obtain reliable broadband surface wave dispersion measurements, *Geophys. J. Int.*, **169**, 1239–1260, https://doi.org/10.1111/j.1365-246X.2007.03374.x, 2007.

Blundy, J., Afanasyev, A., Tattitch, B., Sparks, S., Melnik, O., Utkin, I., and Rust, A.: The economic potential of metalliferous sub-volcanic brines, *R. Soc. Open Sci.*, **8**, 202192, https://doi.org/10.1098/rsos.202192, 2021.

Bogiatzis, P., Ishii, M., and Davis, T. A.: Towards using direct methods in seismic tomography: computation of the full resolution matrix using high-performance computing and sparse QR factorization, *Geophys. J. Int.*, **205**, https://doi.org/10.1093/gji/ggw052, 2016.

Bogiatzis, P., Ishii, M., and Davis, T. A.: The Dulmage–Mendelsohn permutation in seismic tomography, *Geophys. J. Int.*, **218**, 1157–1173, https://doi.org/10.1093/gji/ggz216, 2019.

Bogiatzis, P., Rychert, C. A., and Harmon, N.: Multiple graph realizations method: improving the accuracy and efficiency of the shortest path method through random sampling, *Geophys. J. Int.*, **227**, 669–679, https://doi.org/10.1093/gji/ggab247, 2021.

Chen, Y., Davis, T. A., Hager, W. W., and Rajamanickam, S.: Algorithm 887: CHOLMOD, supernodal sparse Cholesky factorization and update/downdate, *ACM Trans. Math. Softw.*, **35**, 3, 2009.

Copernicus DEM: *Copernicus DEM*, https://doi.org/10.5270/ESA-c5d3d65, 2022.

Engwirda, D.: Generalised primal-dual grids for unstructured co-volume schemes. *J. Comp Phys.*, **375**, 155–176, https://doi.org/10.1016/j.jcp.2018.07.025, 2018.

Forsyth, D. W., and Li, A.: Array analysis of two-dimensional variations in surface wave phase velocity and azimuthal anisotropy in the presence of multipathing interference, in: *Seismic Earth: Array Analysis of Broadband Seismograms*, American Geophysical Union (AGU), https://doi.org/10.1029/157GM06, 2005.

Gallardo, L. A., and Meju, M. A.: Joint two-dimensional DC resistivity and seismic travel-time inversion with cross-gradients constraints, *J. Geophys. Res.*, **109**, B3, https://doi.org/10.1029/2003JB002716, 2004.

GEBCO Bathymetric Compilation Group: The GEBCO_2025 Grid – a continuous terrain model for oceans and land at 15 arc-second intervals, *NERC EDS British Oceanographic Data Centre NOC*, https://doi.org/10.5285/37c52e96-24ea-67ce-e063-7086abc05f29, 2025.

Hu, W., Abubakar, A., and Habashy, T. M.: Joint electromagnetic and seismic inversion using structural constraints, *Geophysics*, **74**, R99–R109, https://doi.org/10.1190/1.3246586, 2009.

Hudson, T. S., Brisbourne, A. M., Kufner, S.-K., Kendall, J.-M., and Smith, A. M.: Array processing in cryoseismology: a comparison to network-based approaches at an Antarctic ice stream, *The Cryosphere*, **18**, 611–628, https://doi.org/10.5194/tc-18-611-2024, 2024.

Hudson, T. S., Kettlety, T., Kendall, J.-M., O'Toole, T., Jupe, A., Shail, R. K., and Grand, A.: Seismic node arrays for enhanced understanding and monitoring of geothermal systems, *The Seismic Record*, **4**, 161–171, https://doi.org/10.1785/0320240019, 2024.

Lesage, P., Heap, M. J., and Kushnir, A.: A generic model for the shallow velocity structure of volcanoes, *J. Volcanol. Geotherm. Res.*, **356**, 114–126, https://doi.org/10.1016/j.jvolgeores.2018.03.003, 2018.

Liu, Y., Dong, L., Wang, Y., Zhu, J., and Ma, Z.: Sensitivity kernels for seismic Fresnel volume tomography. *Geophys.*, **74**, U35–U46, https://doi.org/10.1190/1.3169600, 2009.

Moser, T. J.: Shortest path calculation of seismic rays, *Geophysics*, **56**, 59–67, https://doi.org/10.1190/1.1442958, 1991.

Ryan, G. A.: Reservoir model development based on geophysical information and petrological analysis, *Seismic Research Centre, University of the West Indies*, 2016.

Ryan, G. A. and Shalev, E.: Seismic velocity/temperature correlations and a possible new geothermometer: insights from exploration of a high-temperature geothermal system on Montserrat, West Indies, *Energies*, **7**, 6689–6720, https://doi.org/10.3390/en7106689, 2014.

Ryan, G. A., Peacock, J. R., Shalev, E., and Rugis, J.: Montserrat geothermal system: a 3D conceptual model, *Geophys. Res. Lett.*, **40**, 2038–2043, https://doi.org/10.1002/grl.50489, 2013.

Sánchez-Sesma, F. J., and Campillo, M.: Diffraction of P, SV, and Rayleigh waves by topographic features: a boundary integral formulation, *Bull. Seismol. Soc. Am.*, **81**, 2234–2253, 1991.

Shalev, E., Kenedi, C. L., Malin, P., Voight, V., Miller, V., Hidayat, D., Sparks, R. S. J., Minshull, T., Paulatto, M., Brown, L., and Mattioli, G.: Three-dimensional seismic velocity tomography of Montserrat from the SEA-

CALIPSO offshore/onshore experiment, *Geophys. Res. Lett.*, **37**, 9, https://doi.org/10.1029/2010GL042498, 2010.

Yemane, T., Hudson, T.S., Kendall, J.M., Blundy, J., Tadesse, A.Z., Hammond, J.O., Ayele, A., Ogubazghi, G. and Lapins, S.: Interconnectivity of magmatic and hydrothermal systems of Aluto volcano in the Main Ethiopian Rift inferred from seismicity. *Journal of Geophysical Research: Solid Earth*, *130*(6), p.e2024JB031053. https://doi.org/10.1029/2024JB031053, 2025

Wadge, G., Voight, B., Sparks, R. S. J., Cole, P. D., Loughlin, S. C., and Robertson, R. E. A.: An overview of the eruption of Soufrière Hills Volcano, Montserrat from 2000 to 2010, *Geol. Soc. Lond. Mem.*, **39**, 1–39, https://doi.org/10.1144/M39.1, 2014.

Watanabe, T., Matsuoka, T., and Ashida, Y.: Seismic traveltime tomography using Fresnel volume approach. SEG Technical Program Expanded Abstracts 1999, 1402–1405. https://doi.org/10.1190/1.1820777, 1999.